Bonding Mechanism of Zonal Isolation Materials to Clean and Rusted Casing

Mohammadreza Kamali[1]*, Mahmoud Khalifeh[1], and Arild Saasen[1]

[1]Department of Energy and Petroleum Engineering, University of Stavanger

Summary

In oil and gas and geothermal well construction, a cementitious material is pumped in the wellbore to provide zonal isolation and support the casing during the life cycle of the well. Thus, the cementitious barrier materials must be durable in terms of chemical and mechanical properties and have chemical compatibility with casing pipe. The complex region of casing-cement interface is considered a key parameter to fulfill long-term zonal isolation. This interface must be chemically stable and impermeable to block unwanted formation fluid communication. Shortcomings of conventional Portland cement under operational conditions and increasing sensitivity to its carbon footprint are motivations for a green alternative. Bond strength and sealability of cement with steel surface have been measured previously. But few research works cover surface characterization and morphological analysis of barrier materials and the connected steel surface. This study provides a full picture of selected alternative materials in terms of shear bond strength, hydraulic sealability, and interface morphology analysis of the materials. Materials include API Class G cement, an industrial expansive cement, noncement-based pozzolanic material, geopolymer, and thermosetting resin. Also, clean and rusted steels were considered as a representative for the casing pipe in the field. The samples were prepared under elevated pressure and temperature. The results proved that higher shear bond strength is not an indication of good sealability, and the ingredients used to mix slurries have a critical role in the structure of the interfacial zone between casing and barrier material.

Introduction

In drilling operations, when the casing pipe is placed in an openhole targeting wellbore stabilization, the cementitious slurry is pumped to fill the annular gap between formation rock and the casing, or the area between two casing strings. After placement, the slurry goes through a chain of reactions and hardened to act as barrier. Along with mechanically supporting the casing in place, the barrier material is responsible for sealing the annular gap to prevent fluid flow and also protect the casing from corrosion. Therefore, the barrier material should be impermeable inherently and also bond entirely to the casing to seal-off the annulus.

Through its lifecycle, a well experiences frequent pressure testing and temperature fluctuations, all inducing extra stress in a complex regime at the interface of cement sheath and casing/formation **(Fig. 1).** These loads may have a negative impact on the interfaces of the barrier material with casing steel or the surrounding formation by, for example, forming cracks in the matrix or opening microannular paths at the interfaces. Consequently, the barrier integrity can be compromised in these situations and result in sustained casing pressure (Vrålstad et al. 2019).

The interface of cementitious material with steel casing or different rock formations has been studied previously (Opedal et al. 2014; Lavrov et al. 2017). In Torsæter et al. (2015), the authors examined the gap between cement and pipe using micro-computed tomography and scanning electron microscopy (SEM) techniques. They observed gaps at the interface of steel with cement and reported as micropath for the leakage at the interface. They concluded that cement shrinkage is the main reason for micropath formation. In a recent study (Yang et al. 2021), the authors characterized the interface of steel with cement by 2D and 3D characterization methods. They studied the gap between steel and cement using SEM and in the presence of relative humidity. They concluded that storing and testing conditions have significant impact on the gap size at the interface of cement with steel pipe. Field operations and previous studies confirm that the majority of leaks occur at cement-casing interface rather than at the cement-formation interface (Delabroy et al. 2018; Welch et al. 2020); therefore, after decommissioning of a well, it is common to remove the casing in the section that the permanent barrier is going to be placed (Khalifeh and Saasen 2020).

Different parameters affect the bond strength between cementitious barrier material and casing. Wellbore geometry and eccentricity of casing (Torsæter et al. 2015), mud removal efficiency and mud contamination (Radonjic and Oyibo 2015), mechanical properties of the barrier material and possible chemical interaction at the interface of materials (Kamali et al. 2021), and loading regime at the interface (Tabatabaei et al. 2020) are among the factors affecting bond strength. In oil and gas applications, laboratory tests have been performed to study bonding at the interface of the cement and casing metal, and the results are used for computational simulations. However, the role of interface properties after curing under downhole condition is still a question.

When the cement is placed by the steel casing, a thin protective layer starts to form at their interface. This layer is formed as a result of electrochemical passivation of steel with alkaline pore solution of the cement. The protective layer provides a thermodynamically stable environment for the preexisting mill scale or native iron oxides. However, invasion of corrosive elements such as chloride, sulfates, and carbonates has a destructive effect on the passive film and makes it unstable. After de-passivation, the steel surface will start to corrode, and the corrosion products change the mechanical properties of the interface structure such as strength and sealability. In civil industry, where the case is reinforced concrete, this region is known as a steel-concrete interface and is studied to estimate the service life of the system (Angst et al. 2017). Research studies in civil industry and building materials revealed that the structure and mechanical properties of steel-concrete interface are different compared to the bulk of cement. The accumulation of finer particles and higher concentration of alkaline pore solution at the vicinity of the steel surface leads to the formation of porous hydration products compared to the bulk of cement. Nevertheless, different parameters affect the properties and microstructure of the steel-concrete interface, including but

*Corresponding author; email: mohammadreza.kamali@uis.no

Original SPE manuscript received for review 15 December 2021. Revised manuscript received for review 14 March 2022. Paper (SPE 209812) peer approved 22 March 2022.

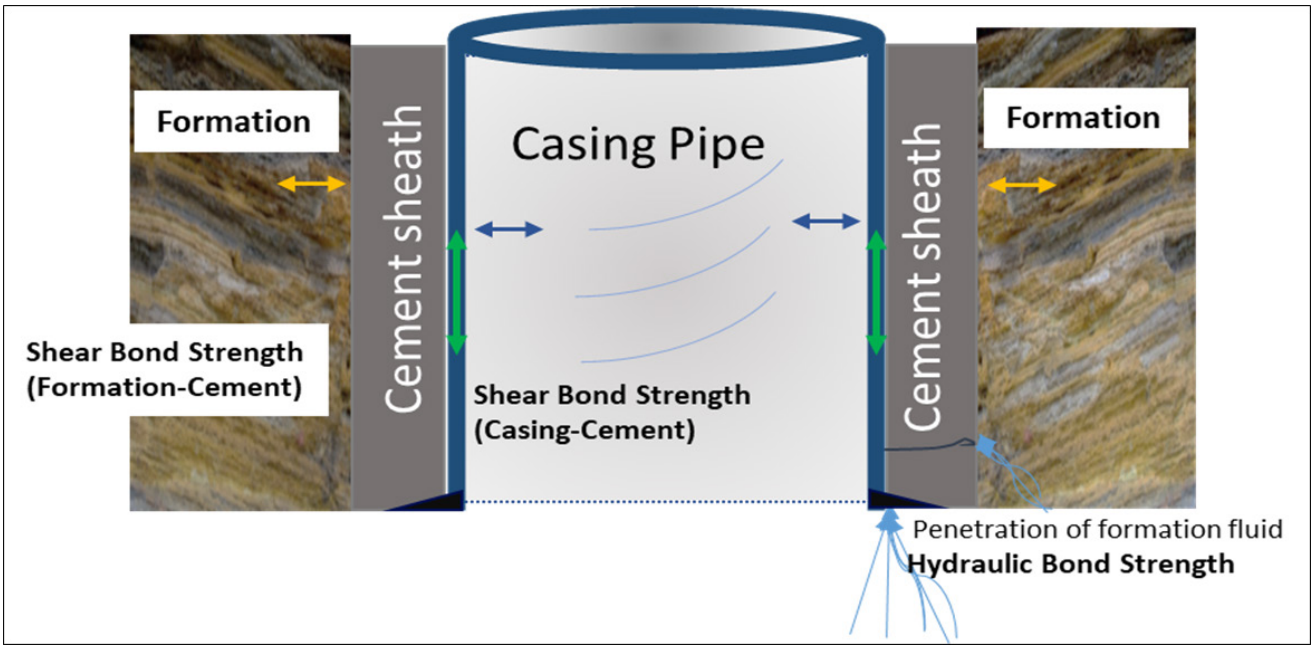

Fig. 1—Complex stress loads on formation, casing pipe, and barrier materials as elements of the well at downhole condition.

not limited to alkaline pore solution composition, binder's chemical composition and fillers, time of exposure, operational condition, and presence of aggressive elements such as weak acids (Zayed 1991; Horne et al. 2007; Angst et al. 2017).

In this study, the objective is to determine the chemical compatibility between alternative setting materials with steel casing. Shear and hydraulic sealability of API neat Class G, an industrial expansive cement, pozzolanic material, inorganic geopolymer, and thermosetting resin were tested. These parameters are measured on both clean and rusted steel to see how existence of rust affects bonding and sealing at the interface. Rheological properties after mixing and mechanical properties of the materials after solidification were studied under the same operational condition, and the results have been already published (Kamali et al. 2021). Although interface analysis has been well-developed in civil industry, to date, there is only limited studies focusing on the interface of barrier materials in oil and gas and geothermal application. In this work, it is attempted to add another dimension to the interface analysis. The morphology and mineralogy of materials at their interface are studied using SEM on polished steel surface and the corresponding setting material.

Setting Barrier Materials. Materials used for cementing operation should fulfill a number of requirements to reduce the risk of uncontrolled release during drilling and production operations (NORSOK-D-010 2013). High strength to withstand mechanical and thermal loads, being chemically compatible with casing material and ensure sufficient bonding to casing and formation, being impermeable, and resisting downhole chemicals are the main criteria for a zonal isolation material. Ordinary Portland cement (OPC) is commonly used for primary cementing and permanent plug and abandonment operations, mainly due to its well-known chemistry and market availability. However, drilling in challenging geographical locations and complex wells highlighted shortcomings with OPC performance in the short- and long-term service life. Among these, low ductility and shrinkage due to hydration reaction induce additional stress on cement matrix. Moreover, contamination with drilling fluids in primary cementing operation can retrograde mechanical strength and negatively affect the hydraulic sealability of cement. The limitations increase the chance of crack and microannular path formation and thus loss of zonal isolation. Possible solutions to overcome shortcomings with barrier material are under development, either by improving the mechanical properties of OPC through application of chemical additives or replacing OPC by other barrier materials for situations that OPC may show restriction. In this study, four different classes of materials have been considered: an industrial expansive cement based on Portland cement, noncement pozzolan-based material, geopolymer, and organic thermosetting resin are selected for measuring the shear bond strength and hydraulic sealability of materials while cured in steel pipes as plug. Following is a brief introduction of the candidate materials.

Industrial Expansive Cement. Previous experimental researches proved that OPC experiences chemical and autogenous shrinkages during the hydration process (Taylor 1997). After solidification, the volume of products is less than reactants, broadly known as chemical shrinkage. One approach to mitigate cement shrinkage is to use expansive agents that expand during hydration. The expansion occurs either by microgas bubble generation or through crystal growth in the matrix of cement (Thomas et al. 2014). One of the most important aspects of using an expanding agent is that expansion should start when shrinkage initiates. Early expansion in cement has no compensation for shrinkage, while very late expansion causes cracks in the cement. Hence, the expansion mechanism must be engineered, for example, by the hybrid use of magnesium oxide with different reactivity (Jafariesfad et al. 2017).

Pozzolanic Material. Pozzolanic materials rich in silica have no cementitious properties on their own. Mixing with alkali hydroxides in an aqueous environment, the mixed slurry can provide cement-like properties (*ASTM C311* 2013). The silica content reacts with calcium hydroxide in the pore solution and forms calcium-silicate-hydrate (C-S-H) phase. In this study, however, the pozzolanic material has no cement in the mix (Kamali et al. 2021). The material has primarily been used as spacer to separate cement slurry from drilling fluid ahead.

Geopolymer. Inorganic polymers known as geopolymers have recently attracted attention due to their short- and long-term stable mechanical properties and lower carbon footprint (Provis 2009). In geopolymerization reaction, long-chain molecules of silicon and aluminum are formed, and the rheological and mechanical properties can be adjusted based on application and the source of raw materials. In these materials, solid phase rich in alumina and silica compounds starts to dissolve in an alkaline-based solution to form Si-O-H and

Al-O-H groups. Later, these single elements, known as monomers, start to orient and reconnect to each other in the mixed slurry and produce oligomers. In the last step, oligomers start to connect and form long-chain molecules and develop 3D aluminosilicate structures.

Thermosetting Resin. Organic thermally activated resin is solidified at a predesigned temperature. Generally, thermosetting resins are particle-free polymers, where, in remedial operations, the liquid polymer is squeezed into microfractures and seals leakage paths (Todorovic et al. 2016). The two factors for designing the thermosetting resin are temperature and the working pressure at which the material will be operated.

Shear Bond and Hydraulic Sealability at the Interface of Isolation Material and Casing. The bond strength between barrier material and casing may be divided into three different categories: (1) shear bond strength, (2) hydraulic bond strength, and (3) tensile bond strength. The scope of this work is to establish the effect of different setting materials in combination with clean and rusty steel on shear bond strength and hydraulic bond strength. Tensile bond strength is not the scope of this article.

Shear Bond Strength. Shear bond strength expresses axial stress at the interface of the barrier material beyond which the casing pipe starts to move within the cement sheath. Failing of the shear bond strength results in lack of mechanical support from the cement for casing pipe, forming microannular path at the interface, and consequently, loss of wellbore integrity. After cementing operation in the field, acoustic logging is the common technique used to verify the quality of barrier material behind the casing string. On the laboratory scale, push-out test is the common method to measure shear bond strength of the material. In this test, a rigid bar with an adequate diameter or a pipe with proper thickness is placed inside the cementitious slurry and the whole system is cured under pressure and temperature. After the desired curing period, the sample is transferred for push-out test, where the bar/pipe is pushed out using compression load. The maximum force at which the pipe starts to slide is reported as a force to break the cement bond (Bearden and Lane 1961). To correlate with different dimensions of the specimen, the force is divided by the contact area between cement and metal to determine the cement support coefficient broadly known as shear bond strength.

Shear bond strength is the function of various factors, for example, friction force at the interface, surface roughness of the casing metal, grain size distribution of the set cement at the interface, and possible chemical interaction due to the various chemical compositions of barrier materials and steel (Lavrov et al. 2019). Nevertheless, decent shear bond strength test results cannot be representative of hydraulic sealability of barrier materials. Cementitious materials can make a strong bond to the casing surface but still leave microannuli at the interface. Micropaths may be formed due to improper placement of the cement, remaining mud between cement and casing, and possible destructive chemical interaction between casing steel and chemical additives in cement in a long-term. Therefore, the hydraulic sealability of setting barrier material can be measured both quantitively and qualitatively by injecting different fluids at the interfaces of cement and casing metal (Ogienagbon et al. 2021; Kamali et al. 2021).

Hydraulic Bond Strength. Hydraulic bond strength shows the integrity at the interface of cement-casing/rock that prevents any fluid flow at boundaries. Early laboratory studies proved that the sealability of the system is the function of cement composition, casing/rock roughness, wetting condition of the casing/rock surface (clean surface–mud-contaminated surface), and interaction between materials at the interface (Evans and Carter 1962). In this study, the hydraulic bond between casing metal and barrier materials is considered. Hydraulic bond strength is measured by curing samples of barrier materials inside a metal pipe representing the casing and then injecting a fluid at the interface of the samples and measuring the fluid flow rate at different injection pressures. As of today, there are several studies discussing the hydraulic sealability of barriers materials trying to understand the performance of systems at downhole conditions (Lecampion et al. 2013; Khalifeh et al. 2018; Corina et al. 2019). As there is no common standard or test procedure to measure the hydraulic sealability test, each study has a designed setup based on the availability of materials and laboratory equipment. Therefore, the results of hydraulic bond studies are valid only for qualitative comparison between the tested materials.

Test Setup and Methodology

The samples of each material were mixed based on the recommended procedure from material suppliers. The samples were cured for seven days under elevated temperature of 90°C. The curing pressure for the hydraulic bond samples was 170 bar. For the shear bond strength test and samples prepared for studying the interface, the pressure was kept at 34 bar due to safety reasons and operation limitations. The procedures for mixing these materials have already been described in detail in our previous study (Kamali et al. 2021). Therefore, **Table 1** only summarizes the ingredient of each material based on the mix design.

	Solid Phase			Liquid Phase by Weight of Solid (BWOS)			Additives (BWOS)					
	API Class G	Naturally Occurring Rock	Glass Bead	Deionized Water (BWOC)	Potassium Silicate Solution	Premixed Resin	Microsilica Solution (50%)	Fluid-Loss Controller	Dispersant	Antifoam	Retarder	Viscosifier
Neat Class G (Dyckerhoff)	790			44								
Expansive cement	790			33			11	2.8	0.5	0.1	0.6	
Pozzolanic material	No information available											
Geopolymer		700			44.5							
Thermosetting resin			720			50						1

Table 1—Mix design of the candidate barrier materials used in this study.

Fig. 2a shows the schematic of shear bond strength test samples. Each sample consists of an inner steel bar with diameter of approximately 50 mm, an outer steel pipe with 150-mm inner diameter, and the annular gap that filled with setting material. The bar was equal to ANSI 4140 P110, which is a common steel used in casing string in field operation in the North Sea. Because of availability and commercial limitations, the outer pipe in shear bond strength samples was selected from a low carbon alloy equal to P235TR1.

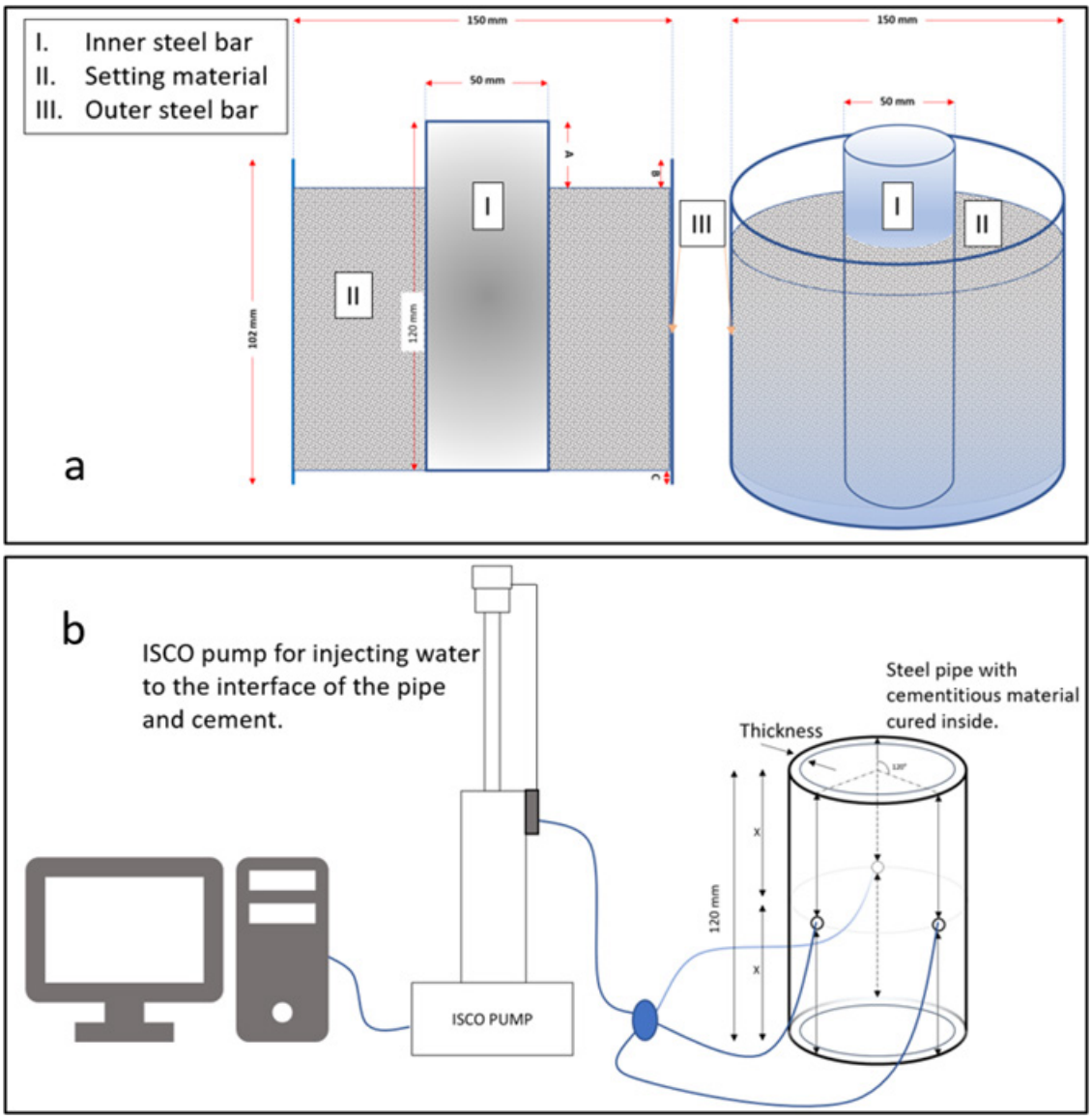

Fig. 2—Schematic of the shear bond strength (a) and hydraulic sealability (b) of the test samples. The shear bond strength test sample includes inner steel bar, setting material, and outer steel pipe. The hydraulic sealability test sample includes a steel pipe with three holes in the middle for injecting fluid.

In **Fig. 2b**, the setup for measuring hydraulic sealability is presented. The samples are cured in steel pipes equal to ANSI 4140 P110 with inner diameter of approximately 36 mm and thickness of 7 mm. The pipes include three holes in the middle facilitating injecting fluid at the interface of steel-setting material.

Shear bond and hydraulic sealability of the materials were measured at both clean and rusted steel surfaces, aiming to see how the corrosion product on the steel can affect the bond strength of materials. Therefore, the same steel materials were immersed in seawater for 14 days. Three samples were prepared per each combination of steel and barrier material for shear bond strength and hydraulic sealability tests. All samples were gradually cooled down after curing and then transferred for testing. The procedure for preparing and testing samples for shear bond and hydraulic bond strength test is described in detail in the previous study (Kamali et al. 2021).

For interface analysis, semicube metals were cut from a 9 $^{5}/_{8}$-in. casing pipe, which was equal to ANSI 4140 L-80 (53 lb/ft) **(Fig. 3).** It has chemical composition similar to P110 and is also commonly used in well construction. **Tables 2 and 3** present the chemical composition and surface roughness of steel metals in this study. There are two main reasons to cure samples on a separate metal. The primary intention was to understand the morphology of cement and steel at the interface and to investigate the possible correlation between such morphology with shear bond and hydraulic sealability of materials. Curing samples inside or outside a pipe surface required application of shear force to separate materials from each other. Hence, it affected the morphology of the surfaces before SEM analysis. Moreover, studying a curved surface of pipe or cement by SEM would be challenging. The samples are exposed to an electron beam inside the microscope. The curved surfaces would not be able to reflect electrons to the detector for imagery purposes.

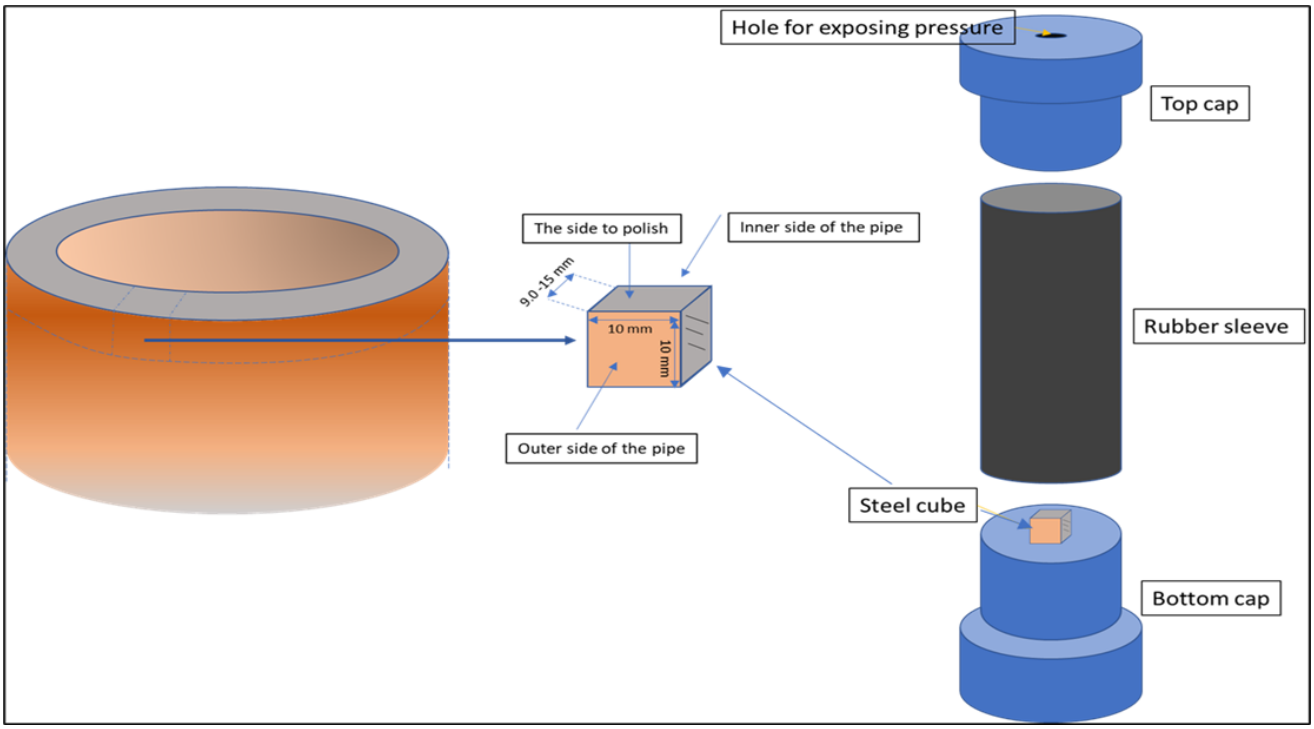

Fig. 3—The setup for curing samples for interface analysis. The dimension of the cube is 10×10×15 mm.

		Chemical Composition % (Max)											
Steel Type	Application	C	Mn	Mo	Cr	Ni	Cu	Ti	P	S	Si	V	Al
4140 P110	SBS* bar-HS† pipe	0.41	0.91	0.23	1.06	0.15	0.2	–	0.011	0.002	0.3	0.013	0.027
P235TR1	SBS outer pipe	0.16	1.2	0.08	0.3	0.3	0.3	0.04	0.025	0.02	0.35	0.02	–
4,140 L80	Surface study	0.43	0.91	0.2	0.9	0.25	0.35	–	0.025	0.025	0.3	–	–

*SBS = shear bond strength.
†HS = hydraulic sealability.

Table 2—Steel metals and the corresponding chemical composition of each metal.

Roughness—Ra (μm)	Clean Surface	Rusty Surface
4140 P110	2.074 ± 0.02	5.788 ± 0.06
P235TR1	1.988 ± 0.01	3.263 ± 0.03
4140 L80 (polished surface)	0.09 ± 0.01	–

Table 3—Roughness of the steel surfaces used in this study in terms of average roughness (Ra).

The cut had the dimension of 15×10×10 mm. One side of the cube was polished with 2,500 grit to remove impurities on the surface. The polished steel was immersed in the slurry and cured for 7 days. **Fig. 3** shows the assembly of the test setup for interface investigation. The surface of steel and the material was removed carefully to avoid any contamination. Both steel metal and barrier material were kept in a desiccator and under vacuum for 1 day and then coated with palladium to study the surface with a scanning electron microscope. Energy-dispersive X-ray spectroscopy (EDS) was used in parallel to SEM, aiming to identify the element distribution on the surface layers of the materials. The microscope used for the SEM and EDS analysis was Zeiss Supra model 35VP.

Results and Discussions

Shear Bond Strength. The shear bond strength test results for both clean steel (top) and rusty surface (bottom) are presented in **Fig. 4.** Because the chemical composition and consequently the morphology of the inner bar and outer pipe surfaces are different, any comparison due to the size and diameter on shear bond strength is irrelevant in this study. Mixing design, curing, and testing conditions were the same for both clean and rusty systems. Therefore, the parameters that take a role in results are the types of materials, change in steel surface roughness, and chemical interaction between rust product and materials after solidification. For the rusted surface, loose particles of the rust can be mixed with the liquid slurry and affect the chemical and mechanical properties of minerals close to the interface with steel.

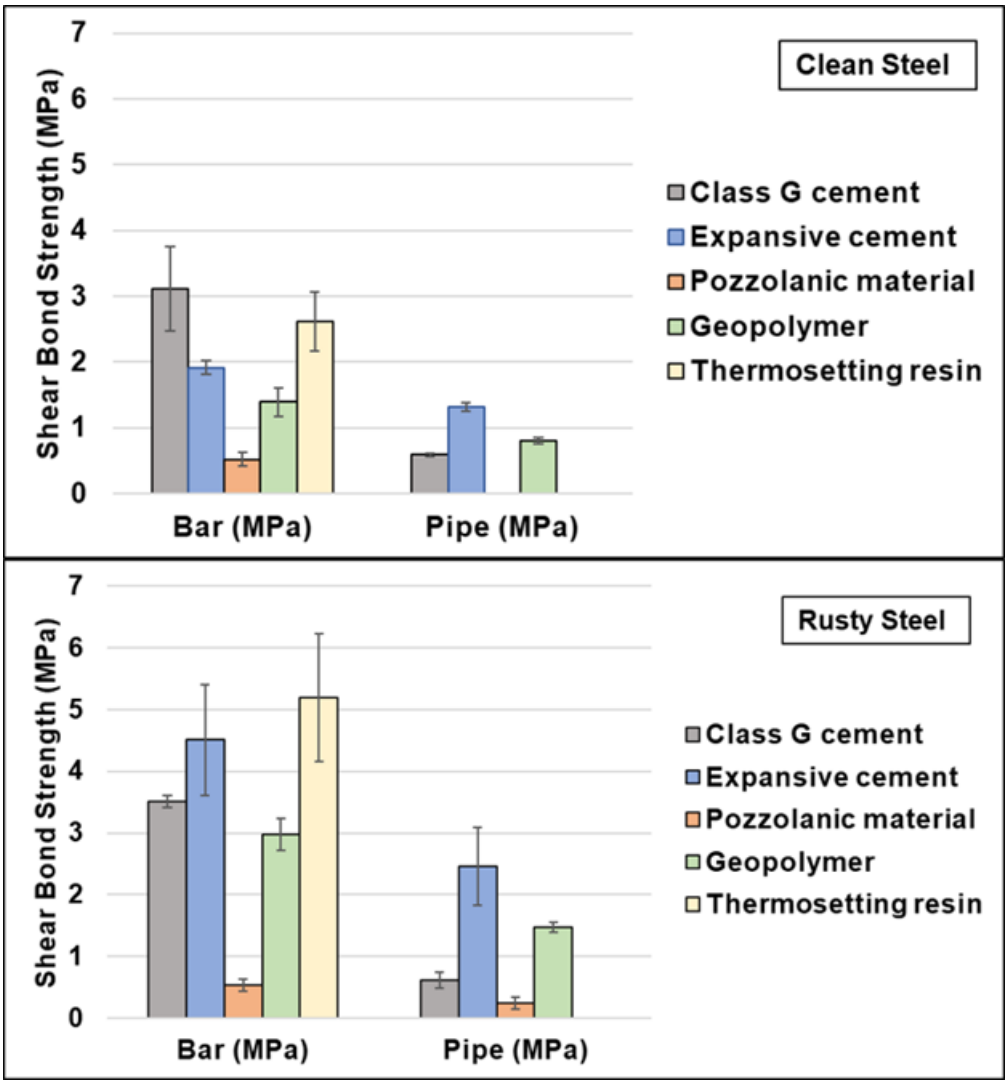

Fig. 4—Shear bond strength test results from push-out test for clean steel surface (top) and rusty surface (bottom).

The thermosetting resin had no bonding to the outer pipe after removal from the curing chamber, neither on the clean steel nor on rusty surfaces. One reason could be due to the higher thermal expansion coefficient of the organic resin compared to the steel. The bond strength of the resin with the middle bar was increased by 100% from 2.6 to 5.2 MPa. It is the highest bond strength measured in this study. Visually inspecting thermosetting resin samples, the sign of adhesion was evident on the bar. However, the high coefficient of thermal expansion can cause bulk shrinkage for temperatures lower than the curing temperature (90°C). Such bulk shrinkage exerted tensile force at outer pipe (concave surface), which resulted in debonding. Similar concept applies on th other side (convex surface); it is expected that thermal shrinkage applies force toward the middle bar. Therefore, the measured shear bond strength was higher than the situation that the test was performed without cooling down.

The pozzolanic material had no bonding to the outer pipe in the clean surface system, while the bond strength reached 0.25 MPa for the rusty surface. Primarily, it was assumed that lack of bonding to the clean outer pipe was because of insufficient mechanical interlock with the smooth surface of the pipe. However, comparing the results at the bar side suggested another hypothesis. The shear bond strength of pozzolanic material remained almost constant at 0.5 MPa for both clean and rusty steel despite the increase in surface roughness by 170%. Therefore, one conclusion is that the pozzolanic material had chemical interaction with the rusty surface of steel that formed different minerals compared to ones at the clean surface. Hence, variation in mineralogy and morphology on the surface directly affects bonding between hardened pozzolanic material and steel surface.

The geopolymer experienced an increase of 100% in shear bond strength at both bar and pipe sides when the clean steel was replaced by rusty steel. The shear bond strength at the bar was increased from 1.5 to 3 MPa and at the pipe, it was increased from 0.75 to 1.5 MPa. Higher bonding at rusty surface is due to both increasing roughness and chemical compatibility with the rust products on the surface. The rust products contain iron oxide. This iron transfers to the geopolymer slurry and generates minerals rich in iron close to the interface. Such structure at the interface may have strong strength which improved shear bond strength. This strong structure, however, has higher permeability. This issue will be discussed in the next section.

Bond strength of the neat Class G cement did not change significantly, neither at the bar nor at pipe sides. Existence of rust on the surface had no impact on the shear bond strength of neat Class G cement. The expansive cement had higher bonding when the surface was covered by rust. The bond strength was increased by about 140% at the bar side, from 1.9 to 4.5 MPa. On the pipe side, the bonding was increased by about 75% and reached 2.5 MPa. The bond strength of expansive cement is the function of both roughness and chemical interaction between the material and rust products, which is similar to the geopolymer.

During push-out tests of the middle bar, it was observed that the matrix of the setting material fails after reaching the maximum load. The failure was in the form of tangential cracks, which appeared at the bottom side of the specimen **(Fig. 5).** In this crack, a part of the matrix is still attached to the bar while the rest is debonded. Formation of such crack is the function of the holder on which the sample stands. In this experimental study, the holder did not cover the whole barrier sheath's bottom area. It was from the outer pipe's inner diameter to one-half the distance between the pipe and the bar. Thus, there was no crack observed on the pipe side.

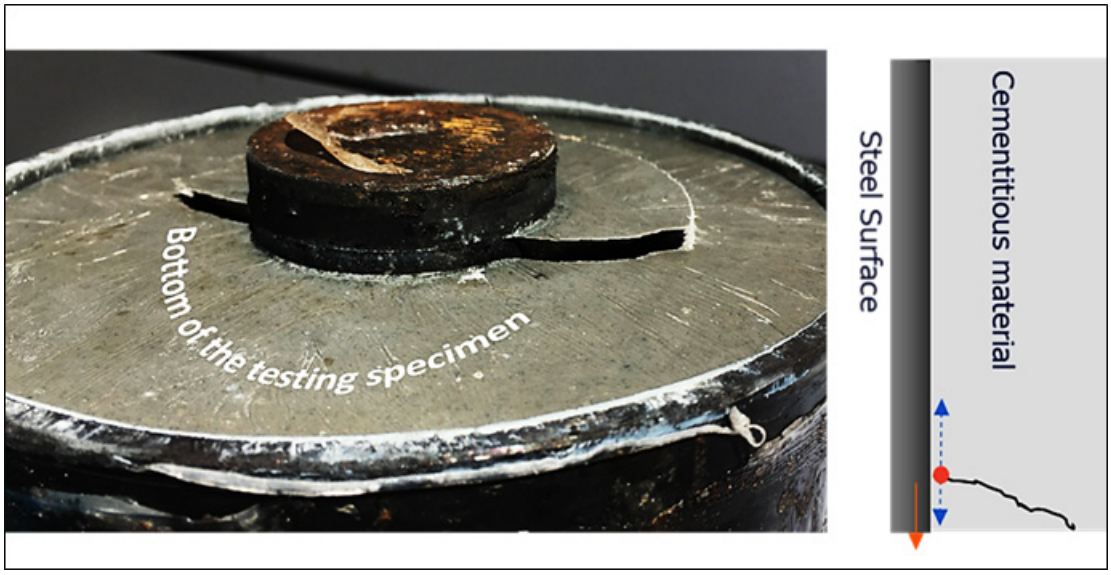

Fig. 5—The tested specimen for shear bond strength. Tangential crack was formed after pushing the middle bar.

One general conclusion is when the interface of the casing pipe and the cement sheath experience axial stress and if the stress is higher than the tensile strength of materials, tangential cracks probably occur in the matrix of the setting barrier material. In this case, low tensile strength is more critical than the shear bond strength. Depending on the wellbore geometry, the crack starts at one point and propagates through the structure of zonal isolation material. Therefore, the ratio of shear bond strength to tensile strength of barrier materials (shear bond strength/tensile strength) was calculated to understand the correlation between the failure mechanisms of the samples. It is presumed that the ratio above unity increases the likelihood of failure due to tensile strength rather than the shear bond. Mechanical properties of the materials with the same mix design were tested earlier up to seven days (Kamali et al. 2020).

In a clean steel system, the ratio for three materials stands around the boundary, which means that the likelihood of failure due to low tensile strength is more than debonding because of shear failing **(Fig. 6).** In this case, development of cracks was observed for all three samples of geopolymer. The ratio for the API Class G cement was almost the same as the geopolymer, but the crack was noted only in two specimens and the depths of the cracks were less than those that occurred in geopolymers. For the expansive cement, although the ratio was aproximately unity, no crack was observed at the bottom of the specimens. In the rusty steel system, the same materials passed the boundary ratio. Therefore, all three samples of geopolymer and two samples out of three for expansive cement and API Class G cement were cracked. Although the ratios for expansive cement and geopolymer were greater than unity at the pipe side, no crack was observed. It is mainly because of the sample holder, which held the samples up to the pipe's inner diameter.

Hydraulic Bond Strength. The goal of hydraulic bond test is to qualitatively compare the sealing ability of alternative setting materials at the clean and rusty steel interfaces. Three tests were performed per each barrier material per casing pipe. **Fig. 7** shows the result of one test for each material per steel surface. The differential pressure trend for samples is also presented in the figure. As no established standard exists to evaluate hydraulic sealability, injection pressure was increased at different steps using the following sequence:

- Increase the injection pressure from ambient to 6.8 bar (100 psi) during 1 minute.
- Hold the pressure for 10 minutes.
- Increase the pressure from 6.8 to 10.2 bar (150 psi) during 1 minute.
- Hold the pressure for 10 minutes.
- Increase the pressure from 10.2 to 13.6 bar (200 psi) during 1 minute.
- Hold the pressure for 5 minutes (where API Class G cement started to leak significantly).
- Increase the pressure from 13.6 bar to 20.4 bar (300 psi) during 1 minute.
- Hold the pressure for 5 minutes.
- Increase the pressure from 20.4 bar to 27.2 bar (400 psi) during 1 minute.
- Hold the pressure for 5 minutes.
- Increase the pressure from 27.2 bar to 34 bar (500 psi) during 1 minute.
- Hold the pressure for about 20 minutes.

Higher injection pressure tests were avoided for safety reasons. Sharp humps in the figures are due to increase of injection flow rate at the interface. Similar to the shear bond strength, the organic thermosetting resin had no bonding to the surrounding steel pipe for the hydraulic sealability test, which is due to the difference in curing temperature (90°C) and testing temperature (25°C), and huge difference between the coefficient of thermal expansion of resin and steel pipes. One mitigating solution to avoid this problem can be curing and testing the material at the same operational condition of pressure and temperature.

The API Class G cement could not hold the hydraulic sealability. The leakage was observed even at early steps of the test. Although the leakage was intensive at the interface of the Class G samples, it was observed that the cement passes the fluid through its matrix

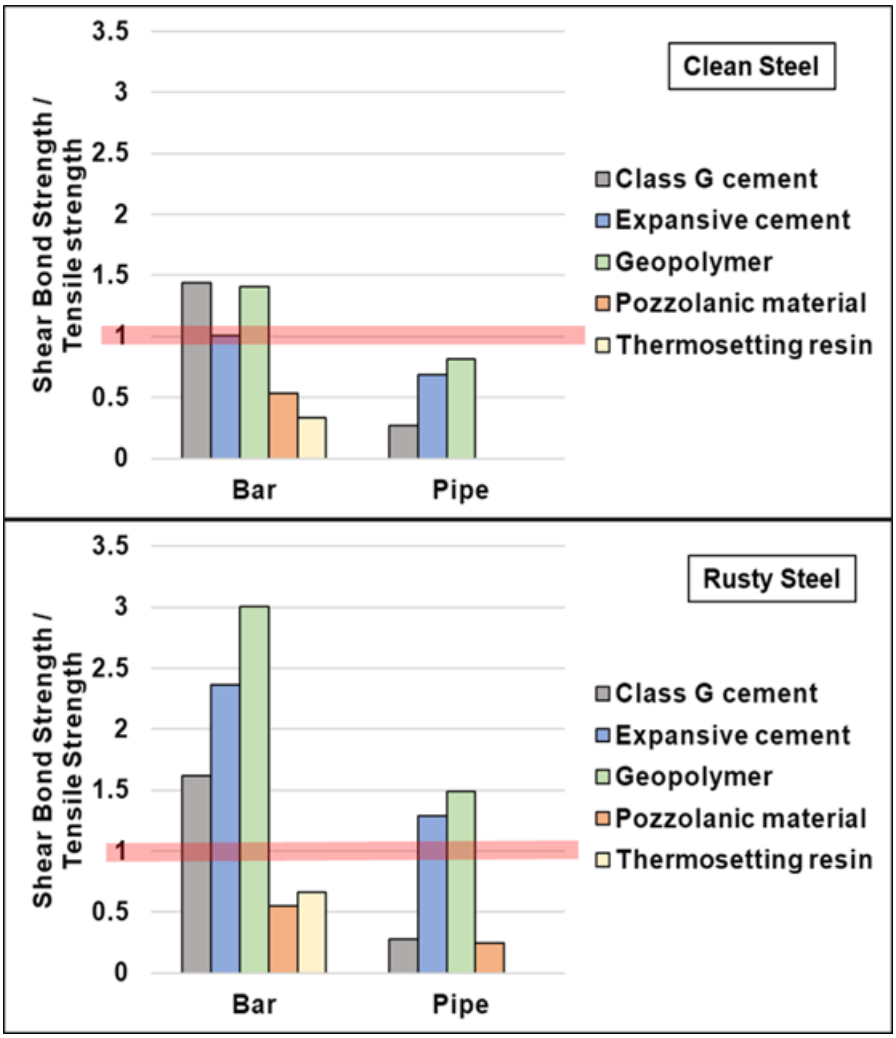

Fig. 6—Ratio of shear bond strength of materials at bar and pipe side to tensile strength of the materials up to 7 days of curing. The ratio was calculated for clean steel (top) and rusty steel surfaces (bottom).

(Fig. 8a). This phenomenon was not witnessed when the expansive cement was used. All three tests with the API Class G cement and clean steel showed the same behavior. Using a rusted surface instead of clean steel had no serious effect on hydraulic sealability of neat Class G cement and steel. Shrinkage of Portland cement is well known both for engineers and scientists (Nelson and Guillot 2006) and is likely the cause of such poor hydraulic sealability. The hydration reaction of cement continues even after the material has been solidified. Unreacted particles in the bulk consume the pore solution, and hence leave empty pores behind. Thus, capillary pressure starts to develop in the matrix and the bulk experiences excess tension due to drainage of the water inside the pores, which affects the volume of bulk to some extent. The change in the volume that occurs as a result of pore water consumption is known as autogenous shrinkage (Henkensiefken et al. 2009). This fact can be attributed to the leakage at the interface of the neat Class G cement samples.

The expansive cement provided a better hydraulic sealability both at clean and rusty surfaces. As there was no leakage observed around samples up to 200 psi, the pressure was increased to 500 psi. The injection flow rate was increased in pressures above 300 psi and the leakage from the bottom of the sample was observed (**Fig. 8b**). This leakage did not occur when the rusty steel pipe was used. Tortuous flow pathways due to increase of surface roughness is one of the main reasons for such performance for expansive cement. Considering the fact that the materials were cured only for 1 week, the expansive cement showed an acceptable hydraulic sealability. The expanding agent used in the mix design improved the performance of the material and compensated autogenous shrinkage of the matrix. Additionally, the microsilica used as an additive to the slurry made a dense structure that prevented fluid flow through the matrix.

The profile of pozzolanic material revealed that despite the good sealability with clean steel, existence of rust at steel surface led to a higher injection flow rate. Moreover, the incompatibility between the pozzolanic material and the rusted surface was apparent at the interface, where the material started to swell in the vicinity of the rusted surface (**Fig. 8c**). The same behavior was observed for samples cured for the shear bond strength test, where the material swelled both at the rusted bar and pipe. Further chemical analysis is required to understand the cause of this observation.

The geopolymer had a better performance when the surface was clean steel. The connections to the testing pipe started to leak at pressures above 400 psi (**Fig. 8d**). Therefore, the injection flow rate for the geopolymer is expected to be less than the values plotted in **Fig. 7**. Existence of rust on the surface had negative impact on the hydraulic sealability at the interface. Although transferring iron from rusted surface to geopolymer improved shear bond strength of geopolymer, it generated minerals with higher permeability that deteriorated hydraulic sealability at the interface. Additionally, since the fluid flow occurred only at the interface with the rusted pipe (but not through the matrix), existence of iron oxide as rust product caused deviation in the designed geopolymerization reaction and formed different minerals compared to the bulk structure.

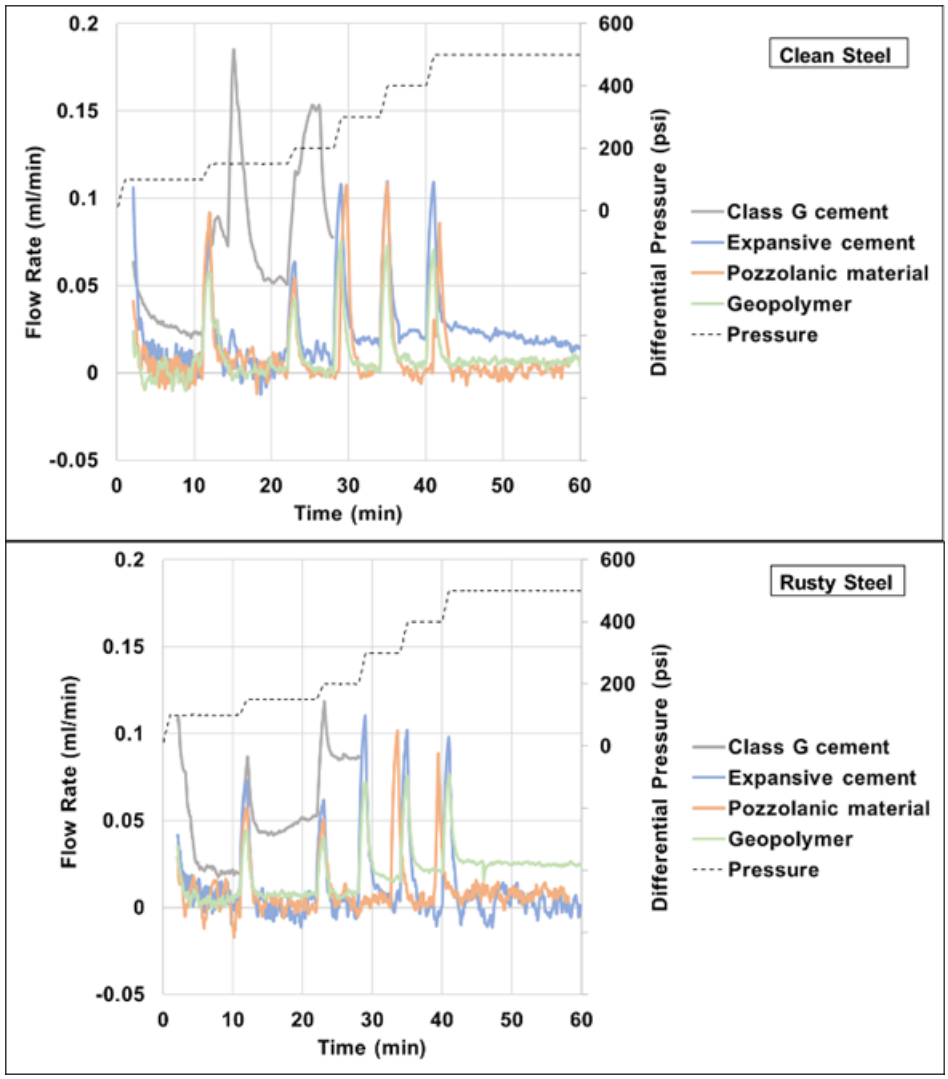

Fig. 7—Hydraulic bond strength test results for clean steel (top) and rusted steel (bottom). Sharp humps in the figures are because of increase in the pressure level across the samples.

Generally, hydraulic sealability of the system is maintained if the material is primarily impermeable and the fluid has no chance to penetrate through the matrix. In the case with API neat Class G cement, the material was permeable to the injected water, while for the rest of materials, no sign of water penetration through the matrices was observed. It is evident that introducing proper additives to the base recipe (such as microsilica in expansive cement) formed a tight structure to fluid migration within the matrix. Additionally, hydraulic sealability at the interface is fulfilled if initially the casing and barrier materials are chemically compatible with each other and can form constructive bonding. Using a proper expansive agent to compensate for possible radial shrinkage of the material keeps the interface against the pipe and reduces the risk of micro annuli formation along the interface.

Steel-Setting Material's Interface. As described in previous paragraphs, properties of the interface between cementitious material and steel are not properly understood. Therefore, the objective of this section is to determine possible interactions at the interface by studying morphology and characterizing minerals after solidification. The steel surface without any coating was considered as metal, and the samples were prepared according to the procedure mentioned in Test Setup and Methodology. The steel was polished, and its surface was washed with acetone, aiming to remove mills and loose particles. The foremost intention was to search for areas on setting materials in which the iron content was higher, indicating chemical interaction between steel and the barrier material. Therefore, the scanning electron microscope was set on backscattered electron mode aiming to search for bright points that are indicators of heavy elements. Later, the test was continued using secondary electron mode of the microscope. **Fig. 9** shows the SEM image and EDS map of Class G cement. The image shows an amorph structure without specific crystalline shape. EDS map analysis of the surface shows area rich in iron (Fe). Studying this zone at higher magnification, no specific structure was observed. The geochemistry analysis of this Class G cement shows about 12% of tetracalcium aluminoferrite (C4AF) in clinker phase, which is the main source of iron in cement powder. Hence, presence of iron on cement surface could not be due to chemical interaction between steel and cement because no free iron exists on the steel surface.

The neat Class G cement developed a porous structure at the interface compared to the other materials **(Fig. 10a).** The surface is covered by C-S-H structure, needle shape ettringite, and a massive amount of hexagonal calcium hydroxide crystals. In general, when the cementitious slurry and steel surface contact each other, a layer starts to form on the steel surface through oxidation of steel. A passive oxidated layer with a thickness range of 3–15 nm protects the steel surface (Chen and Orazem 2016). In this protective layer, alkaline pore

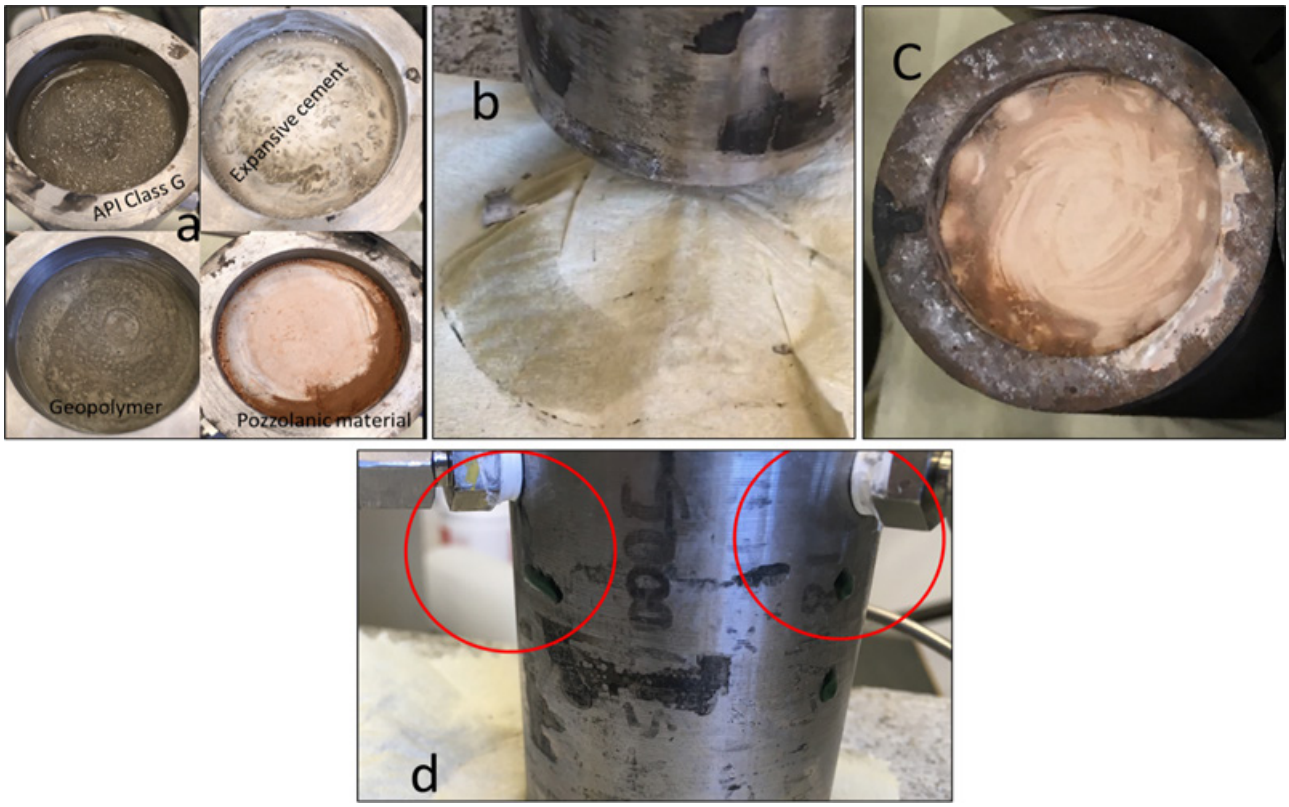

Fig. 8—(a) Fluid penetration through the bulk of API Class G at 150 psi. The bulk of expansive cement, geopolymer, and pozzolanic material was dry at 500 psi. (b) The small leakage from the bottom of the expansive cement. (c) Swelling of the pozzolanic material when it cured inside rusted pipe. (d) Leakage at the connection for the geopolymer samples.

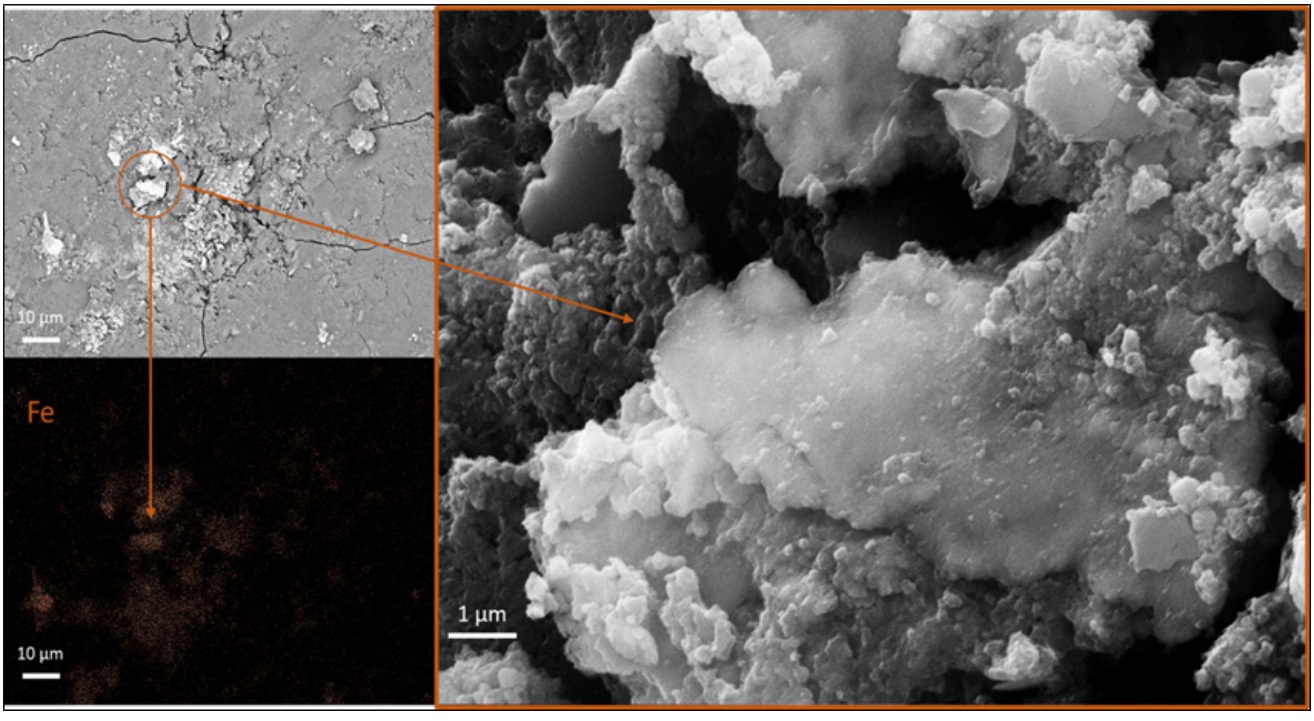

Fig. 9—SEM image of API Class G cement (top left), EDS mapping of iron (bottom left), and secondary electron image at a higher magnification.

solution of the cement [mainly $Ca(OH)_2$] has high concentration. This layer also buffers the pH and acts as a barrier toward destructive corrosion reactions on the steel surface (Page 1975).

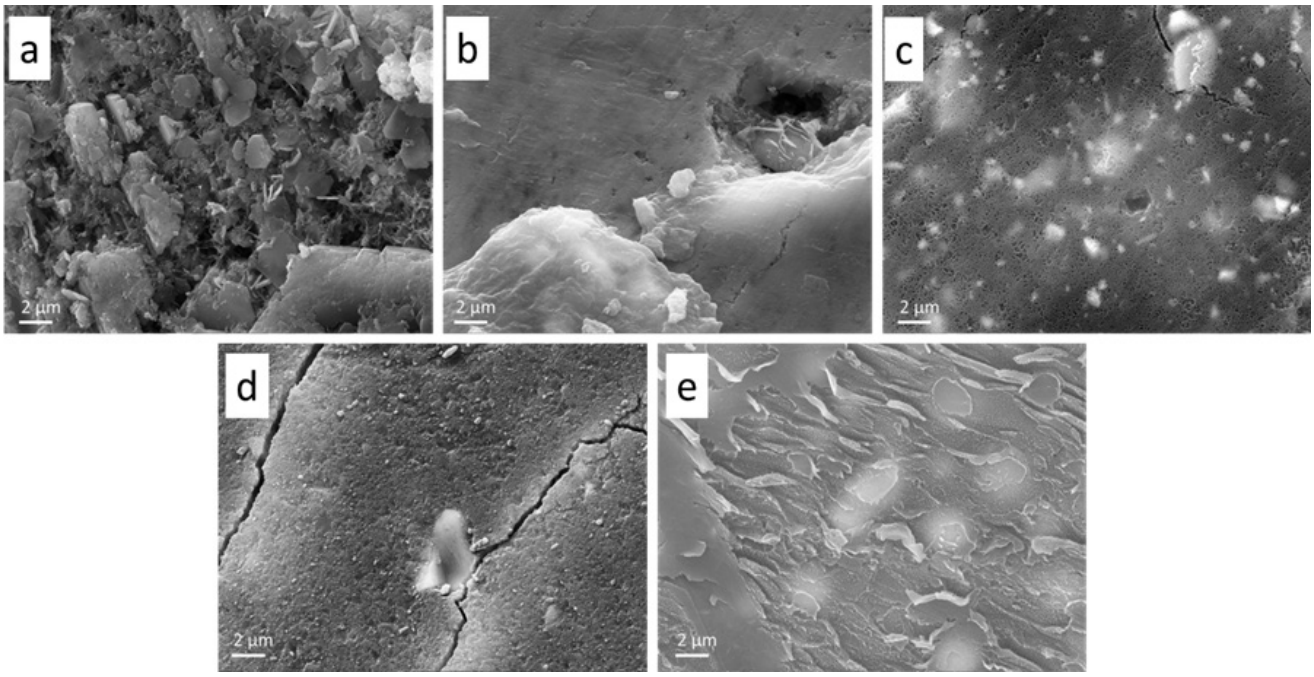

Fig. 10—SEM images of the interface of setting materials with steel surface: (a) Class G cement, (b) expansive cement, (c) pozzolanic material, (d) geopolymer, and (e) thermosetting resin.

The interface has fine and fast reacting particles compared to the cement bulk. Additionally, a higher concentration of $Ca(OH)_2$ at the interface results in the formation of large crystals of calcium hydroxide, which makes the structure more porous. This observation agrees with previous experimental studies (Horne et al. 2007) and also supports the results from hydraulic sealability tests in this study, where the samples started to leak at the interface between neat Class G cement and steel. The corresponding steel surface connected to the Class G is shown in **Fig. 11a.** It is evident that the steel surface is covered with calcium hydroxide fragments and even after removing the cement, the fragments kept their adhesion to the steel surface. From such adhesion of these fragments to steel surface, one can conclude the reason of high shear bond strength of the Class G cement.

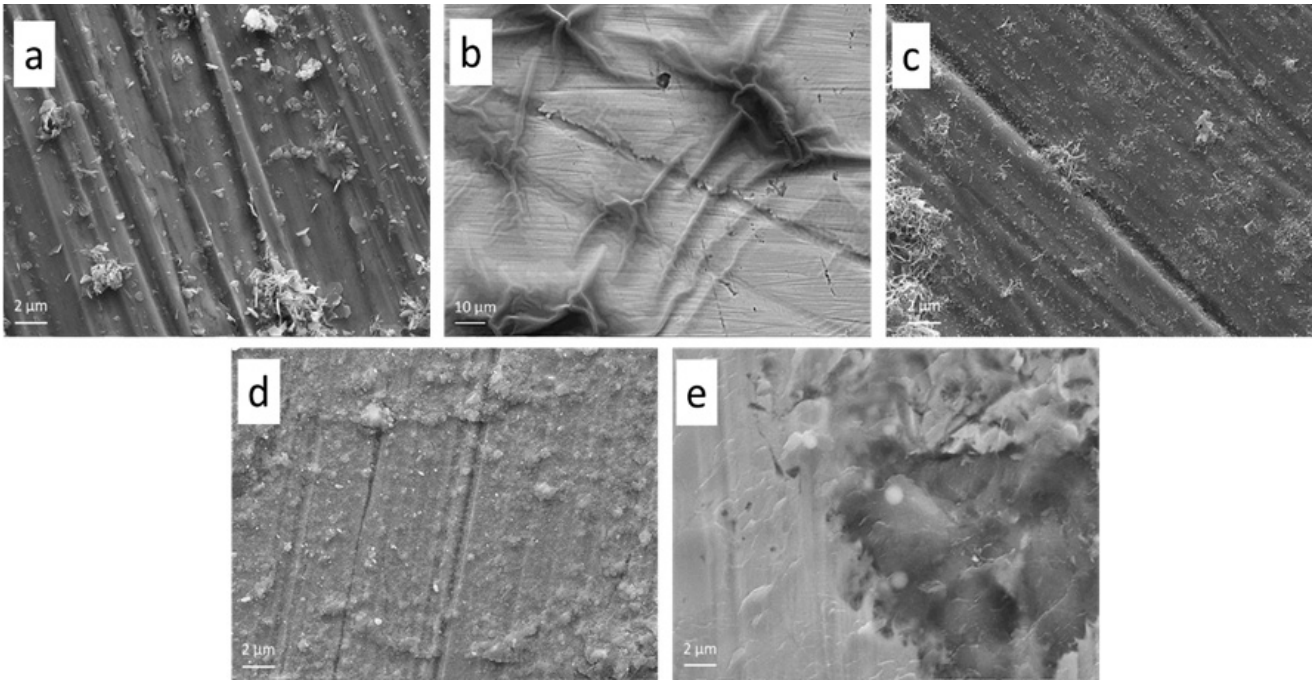

Fig. 11—SEM images of the interface of steel connected to the setting materials: (a) Class G cement, (b) expansive cement, (c) pozzolanic material, (d) geopolymer, and (e) thermosetting resin.

Fig. 10b shows the surface of expansive cement. The uniform surface of the cement proves the decent hydraulic sealability of material. The microsilica used in the mixing recipe filled the pores of the material after solidification and made an impermeable structure. Moreover,

the expanding agents, including magnesium and calcium compounds, inhibited bulk shrinkage of the cement. Consequently, the cement entirely sticks to steel surface with an impermeable interface. In **Fig. 10b**, the ditch formed on the right side showed a high concentration of magnesium, which reveals crystal growth after solidification. However, positioning of expanding agents at the interface may endanger the hydraulic sealability of the system. Lower magnification of the SEM image and the map of elements of the expansive cement are presented in **Fig. 12.** It is evident that the expanding agents have formed crystals rich in magnesium content in some spots. The crystal growth has ruptured the surface and started to rise toward steel. Additionally, the calcium-rich crystals are indicated in the bar configuration, but unlike the Mg-rich crystal, they remain at the same level of surface. This could be either due to the curing period or the confining pressure used for curing samples. Using expanding agents to inhibit shrinkage is critically important. Nonstop crystal growth, especially at the interface of steel and cement, results in forming gaps and debonding due to micropath formation. Hence, the reactivity, particle size, and concentration of expanding agents are the key controlling parameters to get acceptable performance. Accordingly, similar tests on hydraulic sealability and studying the interface after a longer curing period can indicate the mechanism of crystal growth, especially at the interface of cement and casing. **Fig. 11b** presents the surface of steel connected to the expansive cement. The surface was covered with unusual wrinkles. The wrinkles are concentric and branched from spots that were rich in silicate and calcium. As the metal surface for expansive cement was prepared with the same procedure as other materials, such abnormal shape on the surface may be due to the solidification reaction and chemical additives used to mix the slurry. The same pattern was observed in two samples cured for expansive cement. The reason for forming this pattern has remained a question.

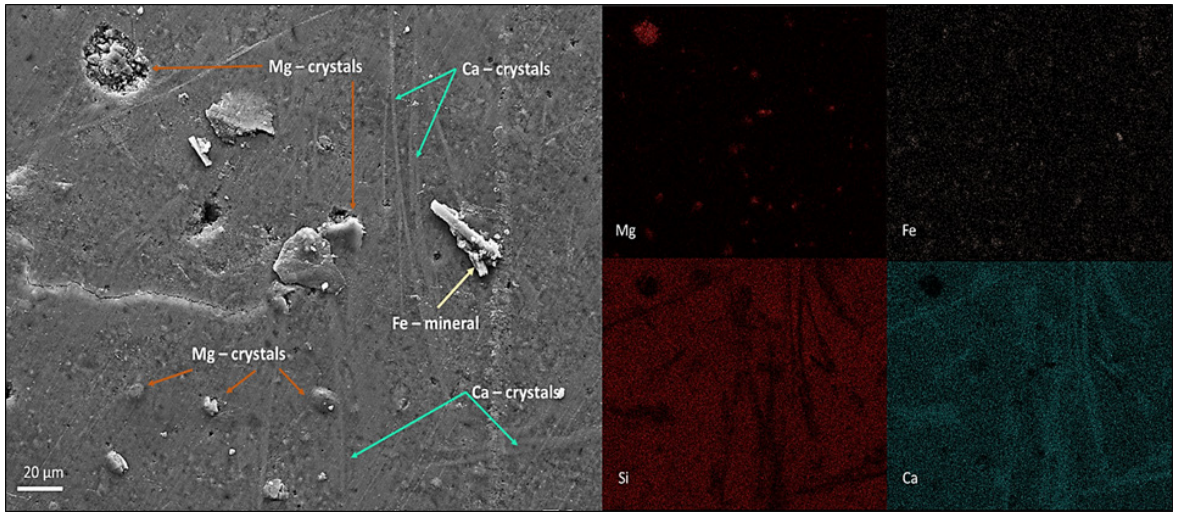

Fig. 12—SEM image, EDS, and elemental map of expansive cement cured on bare steel surface. Magnesium rich area is an indication of expanding agents at the interface.

Fig. 10c shows the surface of pozzolanic material. The SEM image shows relatively porous structure compared to the expansive cement, but the pore sizes are considerably smaller than the cured neat Class G cement. Using backscattered electron, most particles on the surface were bright and shiny, which was an indication of heavy elements **(Fig. 13).** The bright points in the image are ingredients used in the mix design and remained unreacted after solidification. However, using EDS mapping on the surface, only a few points were

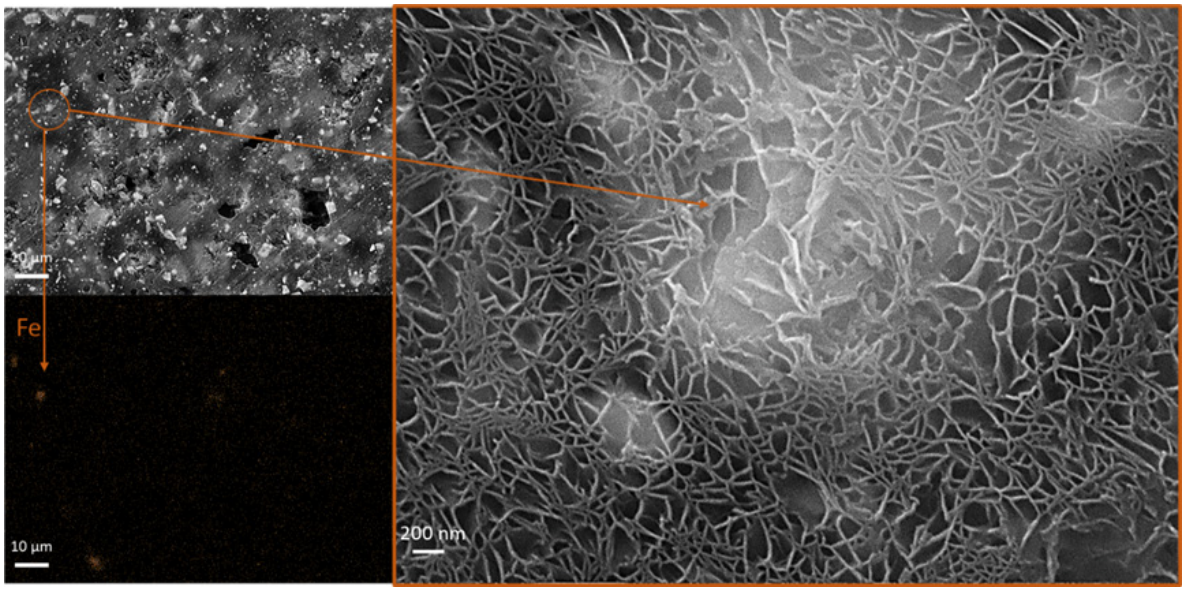

Fig. 13—SEM image of pozzolanic material (top left), EDS mapping of iron (bottom left), and SEM image at higher magnification.

showing iron content in the structure. Unfortunately, mentioning ingredients of the pozzolanic material is prohibited due to commercial requirements. Under higher magnification, the 3D network of the matrix was evident while the crystalline or amorphous structure containing iron was not clear. Correlating SEM images of pozzolanic material with shear bond strength and hydraulic sealability tests, one can conclude that the 3D structure on the surface of the material is not mechanically strong enough to support high shearing forces. However, the existing pores on the surface are disconnected and are able to prevent the injecting flow at the interface. Therefore, a good hydraulic sealability was achieved for the pozzolanic material compared to other alternatives. The corresponding steel connected to the pozzolanic material (**Fig. 11c**) shows structures separated from the barrier material adhered to the steel. The honey comp substance on the left side of the picture matches the porous structure of pozzolanic material. It supports the adhesion between pozzolanic material and steel.

Surface of the geopolymer was investigated in the same way as other materials (**Fig. 10d**). The surface showed a homogeneous structure, which was quite similar to the expansive cement's surface. Such intact structure on surface endures the favorable hydraulic sealability of the material with clean steel. Geopolymerization follows a different path than the hydration reaction of cement. Depending on ingredients and the mix design, the reaction may continue over time so that the unreacted particles (similar to one in the middle of **Fig. 10d**) start to react with alkaline pore solution. Hence, the matrix of the material is always under development. Additionally, fine particles of microsilica used in mixing of slurry act as a bridge between the long chain of aluminosilicate molecules and seals off the matrix. Previous studies reported the same observationthat using microsilica as an additive reduces the porosity of the steel-cement interface (Gjorv et al. 1990). Although the surface is covered by cracks, these cracks are formed after coating and due to vacuum condition of scanning electron microscope chamber.

Using backscattered electron mode, a few bright spots were indicated on the geopolymer surface, and the EDS map analysis revealed the presence of iron in the structure close to the surface **(Fig. 14).** Unlike pozzolanic material and Portland-based systems, the detected spots rich in iron had crystalline structures. This crystalline structure also involves aluminum, silicon, potassium, calcium, and magnesium, which are ingredients used to mix the geopolymer. To identify the exact phase of such crystal on the surface of geopolymer, other techniques and methodologies are required. **Fig. 11d** matches the steel surface connected to the geopolymer. The surface shows a layer of dense and fine product of geopolymerization reaction separated from the matrix and adhered to the steel surface. The profile of the dense structure and its grip on the steel surface supports the hydraulic sealability test results of geopolymer and clean steel pipe. As the shear bond strength of geopolymer was considerably higher than the pozzolanic material, it can be concluded that the structure formed at the interface of geopolymer and steel surface has higher mechanical strength than that of the pozzolanic material.

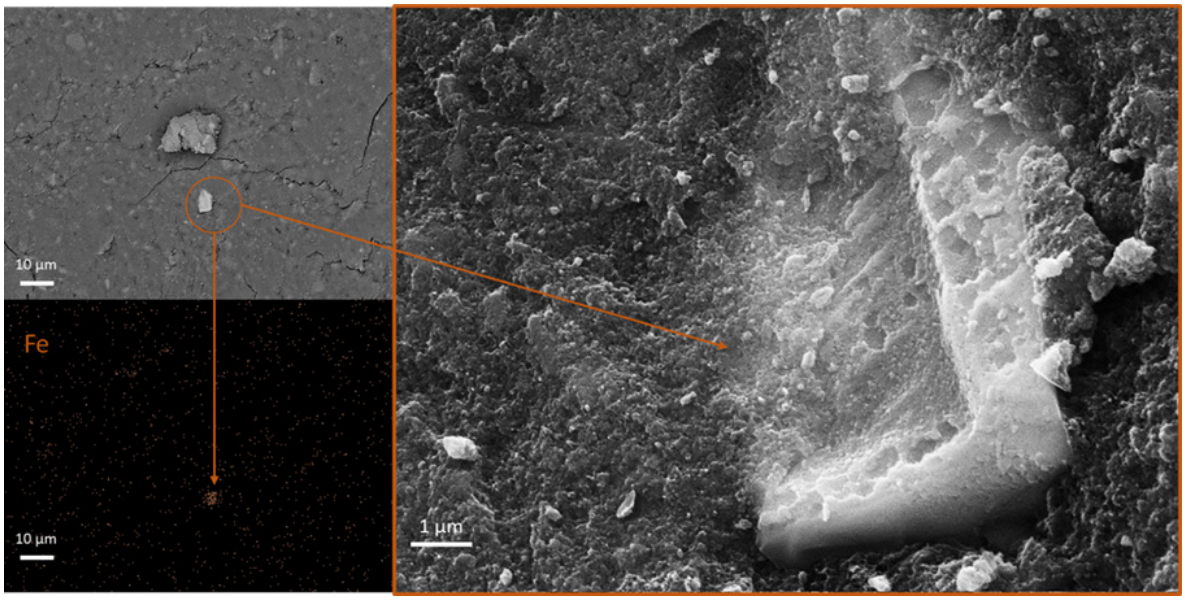

Fig. 14—SEM image of geopolymer (top left), EDS mapping of iron (bottom left), and SEM image at higher magnification.

Figs. 10e and 11e show the thermosetting resin and the corresponding steel surface, respectively. Although the resin failed to resist fluid flow at the interface, it had a good shear bond strength with the inner bar. Scanning the surface, it was only one bright spot on the resin's surface and the EDS map proved iron accumulation on the same region **(Fig. 15).** The spherical-shaped bright spots in the image are glass beads used as filler to increase the density of the slurry. As there was only one point on the entire thermosetting resin showing evidence of iron content, this can be due to errors in sample preparation and the mill scales remained on steel surface transferred to the thermosetting resin. The SEM image of the steel (**Fig. 11e**) shows that the solidified resin has adhered to the surface. In short term, it is an indication of chemical compatibility between the solidified resin and steel, up to 7 days of curing.

In the concrete industry, when cement slurry is placed by the solid steel surface, the particle-size distribution close to the wall is different from the cement matrix. Literature explains this fact as a "wall effect" in which the accumulation of finer particles is higher in slurry close to the wall and larger particles remain at some distance from the steel surface (Scrivener et al. 2004). However, this medium favors porous structure formation in cement-based systems. This theory was supported by observing porous structure in neat Class G cement (**Fig. 10a**). In expansive cement, this zone has become denser, using gas tight additives such as microsilica to the mix, where the calcium hydroxide crystals on the surface were not visible. The wall effect phenomenon was observed clearly in SEM images of the pozzolanic material, geopolymer, and thermosetting resin, where larger particles can be seen under a thin layer from the materials' surfaces.

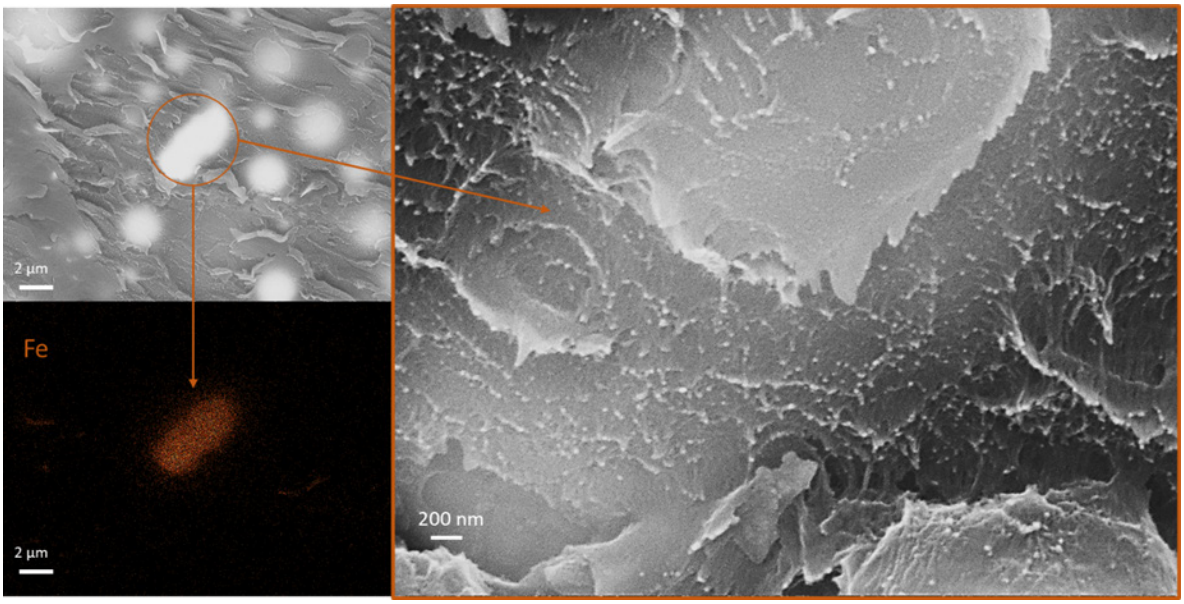

Fig. 15—SEM image of thermosetting resin (top left), EDS mapping of iron (bottom left), and SEM image at higher magnification.

Conclusion

Shear bond and hydraulic sealability of five alternative barrier materials including neat Class G cement, an industrial expansive cement, a noncement-based pozzolanic material, a rock-based geopolymer, and thermosetting resin were tested. Clean and rusty steel surfaces were used as representative of casing in the field. Shear bond strength was increased to various extent when the surface was rusty steel. Change in the surface roughness of steel, chemical interaction between steel and setting materials, and difference in curing and testing conditions have direct impact on the shear bond strength. The API neat Class G cement showed high shear bond strength in the push-out test, but the material failed to provide hydraulic sealability. The pozzolanic material maintained hydraulic sealability during testing, while the shear bond strength was the minimum. No correlation has been found between shear bond and hydraulic sealability.

Existence of rust can directly affect the minerals formed at the interface. Depending on solidification reaction (e.g., hydration, geopolymerization, and polymerization), generated minerals show different chemical and mechanical behavior. The results of shear bond and hydraulic bond strength tests revealed that the industrial expansive cement is more chemically compatible with rust products existing on the surface. EDS mapping of the materials cured on polished steel surface revealed no direct interaction between polished steel surface and setting materials. Existence of iron in the form of rust can have an influence of the minerals formed at the interface. The reactive iron ions existing in rust are transferred to the slurry and react with the material during solidification and become a part of the structure of barrier materials. The rest of the materials were negatively affected by contact to rust. Crystal growth in the matrix of barrier material helps to compensate for possible shrinkages after solidification, but it can also increase the risk of microannular paths at the interface and consequently, loss of zonal isolation.

Acknowledgments

The authors thank Halliburton, Wellcem, and AlTiSS for their technical support and for delivering materials. A special thanks to Johannes Steinnes Jensen, Caroline Einvik, and Emil Surnevik Kristiansen for preparing the test setup for curing samples. The authors also thank Aker BP, ConocoPhillips Norge, TotalEnergies, and the Research Council of Norway for their support through the SafeRock project (#319014—New Cementitious Material for Oil Well Cementing Applications—SafeRock).

Reference

Angst, U. M., Geiker, M. R., Michel, A. et al. 2017. The Steel–Concrete Interface. *Mater Struct* **50** (2): 1–24. https://doi.org/10.1617/s11527-017-1010-1.

ASTM C311, Standard Test Methods for Sampling and Testing Fly Ash or Natural Pozzolans for Use in Portland-Cement Concrete. 2013. West Conshohocken, Pennsylvania, USA: ASTM International.

Bearden, W. G. and Lane, R. D. 1961. Engineered Cementing Operations to Eliminate WOC Time. Paper presented at the Drilling and Production Practice, New York City, New York, USA, 1 January. API-61-017.

Chen, Y.-M. and Orazem, M. E. 2016. Impedance Analysis of ASTM A416 Tendon Steel Corrosion in Alkaline Simulated Pore Solutions. *Corros Sci* **104**: 26–35. https://doi.org/10.1016/j.corsci.2015.11.027.

Corina, A. N., Opedal, N., Vrålstad, T. et al. 2019. Cement Plug Sealing Studies of Silica Cement Systems. Paper presented at the ASME 2019 38th International Conference on Ocean, Offshore and Arctic Engineering, Glasgow, Scotland, UK, 9–14 June. OMAE2019-95928. https://doi.org/10.1115/OMAE2019-95928.

Delabroy, L., Stokkeland, T. A., Åstrand, G. et al. 2018. Perforate Wash and Cement for Large Casing Sizes. Paper presented at the SPE Symposium: Decommissioning and Abandonment, Kuala Lumpur, Malaysia, 3–4 December. SPE-193945-MS. https://doi.org/10.2118/193945-MS.

Evans, G. W. and Carter, L. G. 1962. Bounding Studies of Cementing Compositions to Pipe and Formations. Paper presented at the Drilling and Production Practice, New York City, New York, USA, 1 January. API-62-072.

Gjorv, O. E., Monteiro, P. J., and Mehta, P. K. 1990. Effect of Condensed Silica Fume on the Steel-Concrete Bond. *Mater J* **87** (6): 573–580. https://doi.org/10.14359/2527.

Henkensiefken, R., Bentz, D., Nantung, T. et al. 2009. Volume Change and Cracking in Internally Cured Mixtures Made with Saturated Lightweight Aggregate under Sealed and Unsealed Conditions. *Cem Concr Compos* **31** (7): 427–437. https://doi.org/10.1016/j.cemconcomp.2009.04.003.

Horne, A. T., Richardson, I. G., and Brydson, RMD. 2007. Quantitative Analysis of the Microstructure of Interfaces in Steel Reinforced Concrete. *Cem Concr Res* **37** (12): 1613–1623. https://doi.org/10.1016/j.cemconres.2007.08.026.

Jafariesfad, N., Geiker, M. R., and Skalle, Pål. 2017. Nanosized Magnesium Oxide With Engineered Expansive Property for Enhanced Cement-System Performance. *SPE J.* **22** (5): 1681–1689. SPE-180038-PA. https://doi.org/10.2118/180038-PA.

Kamali, M., Khalifeh, M., Eid, E. et al. 2021. Experimental Study of Hydraulic Sealability and Shear Bond Strength of Cementitious Barrier Materials. *J Energy Resour Technol* **144** (2): 1–33. https://doi.org/10.1115/1.4051269.

Kamali, M., Khalifeh, M., Saasen, A. et al. 2020. Materials for Well Integrity: Characterization of Short-Term Mechanical Properties. Paper presented at the ASME 2020 39th International Conference on Ocean, Offshore and Arctic Engineering, Virtual, 3–7 August. OMAE2020-18623. https://doi.org/10.1115/OMAE2020-18623.

Kamali, M., Khalifeh, M., Saasen, A. et al. 2021. Alternative Setting Materials for Primary Cementing and Zonal Isolation – Laboratory Evaluation of Rheological and Mechanical Properties. *J Pet Sci Eng* **201**: 108455. https://doi.org/10.1016/j.petrol.2021.108455.

Khalifeh, M., Hodne, H., Saasen, A. et al. 2018. Bond Strength Between Different Casing Materials and Cement. Paper presented at the SPE Norway One Day Seminar, Bergen, Norway, 18 April. SPE-191322-MS. https://doi.org/10.2118/191322-MS.

Khalifeh, M. and Saasen, A. 2020. *Introduction to Permanent Plug and Abandonment of Wells*. Berlin, Germany: Springer Nature. https://doi.org/10.1007/978-3-030-39970-2.

Lavrov, A., Bhuiyan, M., and Stroisz, A. 2019. Push-out Test: Why Bother? *J Pet Sci Eng* **172**: 297–302. https://doi.org/10.1016/j.petrol.2018.09.067.

Lavrov, A., Gawel, K., Stroisz, A. et al. 2017. Failure Modes in Three-Point Bending Tests of Cement-Steel, Cement-Cement and Cement-Sandstone Bi-Material Beams. *Constr Build Mater* **152**: 880–886. https://doi.org/10.1016/j.conbuildmat.2017.07.017.

Lecampion, B., Bunger, A., Kear, J. et al. 2013. Interface Debonding Driven by Fluid Injection in a Cased and Cemented Wellbore: Modeling and Experiments. *Int J Greenh Gas Control* **18**: 208–223. https://doi.org/10.1016/j.ijggc.2013.07.012.

Nelson, E. B. and Guillot, D. 2006. *Well Cementing*. Houston, Texas, USA: Schlumberger.

NORSOK-D-010. 2013. *Well Integrity in Drilling and Well Operations*. Norway: Standard Norway. https://www.npd.no/globalassets/1-npd/regelverk/skjema/bronnregistreing/eng/norsok-d-010-2013-well-integrity-and-well-operations-rev-4.pdf.

Ogienagbon, A., Khalifeh, M., Yang, X. et al. 2021. Characterization of Microannuli at the Cement-Casing Interface: Development of Methodology. Paper presented at the Abu Dhabi International Petroleum Exhibition & Conference, Abu Dhabi, UAE, 15–18 November. SPE-207581-MS. https://doi.org/10.2118/207581-MS.

Opedal, N., Todorovic, J., Torsaeter, M. et al. 2014. Experimental Study on the Cement-Formation Bonding. Paper presented at the SPE International Symposium and Exhibition on Formation Damage Control, Lafayette, Louisiana, USA, 26–28 February. SPE-168138-MS. https://doi.org/10.2118/168138-MS.

Page, CL. 1975. Mechanism of Corrosion Protection in Reinforced Concrete Marine Structures. *Nature* **258** (5535): 514–515. https://doi.org/10.1038/258514a0.

Provis, J. L. and Deventer, J. an. 2009. *Geopolymers: Structures, Processing, Properties and Industrial Applications*. Amsterdam, Netherlands: Elsevier.

Radonjic, M. and Oyibo, A. 2015. Comparative Experimental Evaluation of Drilling Fluid Contamination on Shear Bond Strength at Wellbore Cement Interfaces. *World J Eng* **11** (6): 597–604. https://doi.org/10.1260/1708-5284.11.6.597.

Scrivener, K. L., Crumbie, A. K., and Laugesen, P. 2004. The Interfacial Transition Zone (ITZ) Between Cement Paste and Aggregate in Concrete. *Interface Sci* **12** (4): 411–421. https://doi.org/10.1023/B:INTS.0000042339.92990.4c.

Tabatabaei, M., Dahi Taleghani, A., and Alem, N. 2020. Measurement of Mixed Mode Interfacial Strengths with Cementitious Materials. *Eng Fract Mech* **223**. https://doi.org/10.1016/j.engfracmech.2019.106739.

Taylor, H. F. 1997. *Cement Chemistry*. London, UK: Thomas Telford Pub.

Thomas, J., Musso, S., Catheline, S. et al. 2014. Expanding Cement for Improved Wellbore Sealing: Prestress Development, Physical Properties, and Logging Response. Paper presented at the SPE Deepwater Drilling and Completions Conference, Galveston, Texas, USA, 10–11 September. SPE-170306-MS. https://doi.org/10.2118/170306-MS.

Todorovic, J., Raphaug, M., Lindeberg, E. et al. 2016. Remediation of Leakage through Annular Cement Using A Polymer Resin: A Laboratory Study. *Energy Procedia* **86**: 442–449. https://doi.org/10.1016/j.egypro.2016.01.045.

Torsæter, M., Todorovic, J., and Lavrov, A. 2015. Structure and Debonding at Cement–Steel and Cement–Rock Interfaces: Effect of Geometry and Materials. *Constr Build Mater* **96**: 164–171. https://doi.org/10.1016/j.conbuildmat.2015.08.005.

Vrålstad, T., Saasen, A., Fjær, E. et al. 2019. Plug & Abandonment of Offshore Wells: Ensuring Long-Term Well Integrity and Cost-Efficiency. *J Pet Sci Eng* **173**: 478–491. https://doi.org/10.1016/j.petrol.2018.10.049.

Welch, N. J., Frash, L. P., Harp, D. H. et al. 2020. Shear Strength and Permeability of the Cement-Casing Interface. *Int J Greenh Gas Control* **95**: 102977. https://doi.org/10.1016/j.ijggc.2020.102977.

Yang, X., Kuru, E., Gingras, M. et al. 2021. Characterization of the Microstructure of the Cement/Casing Interface Using ESEM and Micro-CT Scan Techniques. *SPE J.* **26** (3): 1131–1143. SPE-204227-PA. https://doi.org/10.2118/204227-PA.

Zayed, A. M. 1991. The Nature of the Concrete-Steel Rebar Interface in Plain and Silica Fume Concrete. *MRS Online Proceedings Library (OPL)*: 245. https://doi.org/10.1557/PROC-245-341.